ACS APPLIED MATERIALS & INTERFACES

Research Article

www.acsami.org

Gold-Decorated Titania Nanotube Arrays as Dual-Functional Platform for Surface-Enhanced Raman Spectroscopy and Surface-Assisted Laser Desorption/Ionization Mass Spectrometry

Syuhei Nitta,[†] Atsushi Yamamoto,[†,‡] Masahiro Kurita,[†] Ryuichi Arakawa,[†] and Hideya Kawasaki*[,†]

[†]Department of Chemistry and Materials Engineering, Faculty of Chemistry, Materials and Bioengineering, Kansai University, 3-3-35 Yamate-cho, Suita-shi, Osaka 564-8680, Japan

[‡]Osaka City Institute of Public Health and Environmental Sciences, 8-34, Tojocho, Tennojiku, Osaka, Japan

Supporting Information

ABSTRACT: In this report, we demonstrate gold-decorated titania nanotube arrays (Au-TNA substrate) as a dual-functional platform for surface-enhanced Raman spectroscopy (SERS) and surface-assisted laser desorption/ionization mass spectrometry (SALDI-MS). The Au nanoparticles are grown on the substrate using vapor deposition of Au. The resulting substrates perform better than Au colloids in terms of the reproducibility of the SERS measurements, long-term stability of the fabricated structures, and clean surface of the Au. The nanostructure of the Au-TNA substrate was designed to optimize the SALDI-MS and SERS performance. Excellent reproducibility of the SERS measurements using the Au-TNA substrate was obtained, with a standard error less than 6 %. SALDI activity was also demonstrated for the same Au-TNA substrates. Finally, the Au-TNA substrate was used for combined SERS and SALDI-MS analysis (i) to discriminate the structural isomers of pyridine compounds (*para-*, *meta-*, and *ortho-*pyridinecarboxylic acid) and (ii) to detect polycarbamate, a dithiocarbamate fungicide. These results are difficult to obtain using either approach alone.

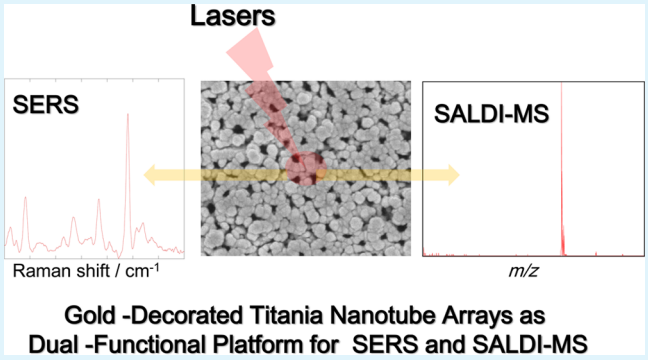

KEYWORDS: *surface-enhanced Raman spectroscopy, surface-assisted laser desorption/ionization mass spectrometry, titania nanotubes, gold*

INTRODUCTION

Plasmonic gold and silver nanoparticles have unique size-dependent physiochemical properties, along with unique physical properties depending on the morphology (i.e., the shape and dimensions), composition (i.e., whether the nanoparticles are alloys or metals), and agglomeration of nanoparticles.[1−3] These properties of metal nanoparticles have led to the development of surface-assisted analytical methods using metal nanoparticles for biological, environmental and food safety analysis, such as surface-enhanced Raman spectroscopy (SERS),[4−8] localized surface plasmon resonance (LSPR) sensing,[9−11] and surface-assisted laser desorption/ionization mass spectrometry (SALDI-MS).[12−19] These analytical methods have found widespread use for direct and label-free analysis in biomedicine, multiplex high-throughput screening, pollutant monitoring, and molecular and materials characterization.[4−19] Furthermore, combinations of surface-assisted analytical methods with other analytical methods have shown good synergies,[5] such as LSPR/LDI-MS[20−22] and secondary ion mass spectrometry (SIMS)/SERS.[23]

SALDI-MS is a surface-assisted analytical method based on mass spectrometry in which metal (Au, Ag) nanoparticles act as the LDI-assisting matrix.[12−19] SALDI-MS is useful for the identification of analytes based on their molecular masses and allows different species to be distinguished from one another. However, it is difficult to identify structural isomers with the same mass using SALDI-MS. In some cases, SALDI-MS has problems with suppression of the analyte ion signals due to the coexistence of compounds with high ionization efficiency. SERS is another surface-assisted analytical technique based on vibrational spectroscopy in which the Raman scattering by molecules adsorbed on the surfaces of metal (Au, Ag) nanoparticles is enhanced by nanoscale surface effects.[4−8] SERS is rapid and nondestructive and offers information about the chemical functional groups, orientation, and interactions of the adsorbed molecules.[4−8] On the other hand, SERS analysis sometimes involves problems with the interpretation of Raman spectra, since clear assignment of the measured Raman bands to specific vibrations is not always possible. Thus, the combination of SERS with SALDI-MS would have great

Received: March 4, 2014
Accepted: April 14, 2014
Published: April 14, 2014

potential for a variety of applications. In particular, enhanced Raman and SALDI-MS signals obtained using Au or Ag nanoparticles could yield complementary information when the two methods are applied to the same sample region. This could provide results that are difficult to ascertain using either approach alone. There are a number of reports on Au or Ag nanoparticles with high SERS activity[4−8] or high SALDI activity individually.[12−19] However, the literature concerning nanostructured metal substrates with dual-functional SERS/SALDI activity is limited, for example, to work on Ag colloids by Nie et al.[24]

The purpose of this paper is to fabricate such nanostructured metal substrates with dual-functional SERS/SALDI activity. For this purpose, the substrates must support a SERS-enhancement medium while simultaneously enhancing the laser-induced desorption and ionization for SALDI. Herein, we report that Au-decorated titania nanotube arrays (Au-TNA substrate) act as such dual-functional SERS/SALDI-active substrates. In place of an Au colloidal solution (prepared by adding Au colloids onto the TNA), we used an Au-TNA substrate prepared by vapor deposition of Au to achieve better reproducibility, long-term stability, and a cleaner surface of the Au. The SERS signal was optimized by varying the amount of Au deposited on the TNA, and ultimately high SERS activity and excellent reproducibility of results were obtained, with a standard error less of than 6%. The same Au-TNA substrates also showed SALDI activity. The specific ways in which the amount of Au affects the SERS and SALDI activity by changing the morphology of the materials was also examined. Finally, the Au-TNA substrate was used for a combined SERS with SALDI-MS analysis (i) to discriminate the structural isomers of pyridine compounds (*para*-, *meta*-, and *ortho*-pyridinecarboxylic acid) and (ii) to detect polycarbamate, a dithiocarbamate fungicide.

EXPERIMENTAL METHODS

Reagents. Methanol, 46% hydrofluoric acid (HF), hydrogen tetrachloroaurate(III) tetrahydrate ($HAuCl_4{\cdot}4H_2O$), ammonium sulfate ($(NH_4)_2SO_4$), rhodamine 6G (R6G), 4-aminothiophenol(4-ATP), *para*-pyridinecarboxylic acid (*p*-Py), *meta*-pyridinecarboxylic acid (*m*-Py), *ortho*-pyridine carboxylic acid (*o*-Py), angiotensin II (Ang. II), and trifluoroacetic acid (TFA) were purchased from Wako Pure Chemicals (Osaka, Japan). Au foil (99.9 %) with a thickness of 0.1 mm was purchased from Sigma-Aldrich. Polycarbamate was purchased from Hayashi Chemical (Osaka, Japan). Titanium foils (0.1 mm thick, 99.5% pure) were purchased from Nilaco Co. (Tokyo, Japan).

Preparation of the Titania Nanotube Array (TNA). Titanium foil (0.1 mm thick, 99.5% pure) was cut into 1.5 cm × 1.5 cm squares, which were cleaned with methanol in an ultrasonic bath, rinsed with deionized water, and finally dried in air. Then, 100 mL of a 1 M aqueous $(NH_4)_2SO_4$ solution containing 0.46 wt % HF was used as an electrolyte for potentiostatic anodization (7651, Yokogawa Co, Japan) using a Pt cathode to prepare a TNA with a tube diameter of about 100 nm and a tube length of about 500 nm.[25−32] The distance between electrodes was 20 mm. The electrochemical treatment consisted of a potential ramp from the open circuit potential (OCP) to 20 V at a sweep rate of 0.025 V/sec and subsequent holding at 20 V for 120 min. After the electrochemical treatment, the TNA substrates were rinsed with deionized water and dried in nitrogen gas. To obtain an anatase-type TNA, thermal annealing was conducted at 500 °C for 3 h in ambient air using a KDF-S 70 thermal annealer (Denken Co, Japan). In this process, the annealing temperature was increased up to 500 °C at a heating rate of 30 °C/min.

Gold Deposition on the TNA. Au was deposited on the TNA substrate to obtain the Au-TNA substrate using a commercially available magnetron sputter vapor deposition (MSVD) device (MSP-1S, Vacuum Device Inc., Ibaragi, Japan) at a discharge current of 45 mA. Au-TNA substrates with differing amounts of deposited Au were prepared by changing the sputtering time. The average amount of the Au deposited per cm^2 was estimated from the mass gains of the samples after the metal deposition process divided by the surface area of the TNA. Herein, we assumed the surface area of TNA is 8 cm^2 per 1 cm × 1 cm square substrate, based on previously reported values.[31]

Scanning Electron Microscopy (SEM). SEM (JEOL JSM-6700 FE-SEM) was used to observe the surface structures at an accelerating voltage of 5.0 kV.

Atomic Force Microscopy (AFM). AFM images of the substrates were acquired at room temperature using a NanoScope IIIa (Veeco) in tapping mode. The AFM images were obtained at a scan rate of 0.5 Hz using silicon tips with a nominal spring constant of 42 N m^{-1} in air.

X-ray Diffraction (XRD). The phase of the Au deposited on the TNA was identified by X-ray diffraction (XRD; Bruker D2 Phaser Table-top Diffractometer) using Cu Kα radiation at 30 kV and 10 mA with a step size of 0.02° (θ) and step time of 4 s between 15 and 100° (θ). Data were collected at room temperature.

SERS. The Au-TNA substrates were immersed in an analyte solution for 30 min, washed with deionized water, and dried by flowing N_2 before the SERS measurement. We used R6G and 4-ATP as the model analytes for SERS measurements. SERS spectra were recorded using a Raman spectrometer (EZ Raman-H, Enwave Optronics, Inc.) at room temperature. All measurements were made with a back-scattering geometry using the Raman spectrometer with an excitation wavelength of 785 nm, a resolution of 6.5 cm^{-1}, a beam diameter of 35 μm, laser beam exposure time of 5 s. The peak laser power was 100 mW.

SALDI-MS. The Au-TNA substrates were fixed to a stainless-steel sample plate using double-sided conductive carbon tape. A 0.5 μL sample solution of Ang. II containing a cationization agent (0.1% TFA) was spotted on this substrate and dried under reduced pressure. The SALDI mass spectra were obtained in the linear mode using an AXIMA CFR TOF mass spectrometer (Shimadzu, Kyoto, Japan) with a pulsed nitrogen laser (337 nm). One hundred laser shots were used to acquire the mass spectra. The analyte ions were accelerated at 20 kV under delayed extraction conditions.

Combined SERS and SALDI-MS Analysis Using the Same Au-TNA Substrate. For the combined analysis, the SERS measurements were conducted first, and then the SALDI activity was evaluated by performing SALDI-MS using the same substrate.

I. Pyridine Carboxylic Acids. The Au-TNA substrate was immersed in an aqueous solution of 1 mM pyridine carboxylic acid (*p*-Py, *m*-Py, or *o*-Py) for 30 min, washed with deionized water, and dried by flowing N_2 before the SERS measurement. The SERS spectra were recorded using a Raman spectrometer at room temperature. After the SERS measurement, the same Au-TNA substrate was fixed to a stainless-steel sample plate using double-sided conductive carbon tape, and SALDI-MS was performed.

ii. Polycarbamate. First, solid polycarbamate (5 mg) was introduced into 10 mL of water and then sonicated for 3 min. A white suspension was obtained, which was then kept at 25 °C for 1 day. A saturated aqueous polycarbamate solution was obtained from the resulting supernatant of the mixture. The Au-TNA substrate was immersed in the saturated polycarbamate solution for 30 min, then washed with deionized water three times, and finally dried by flowing N_2 before the SERS measurement. The SERS spectra were recorded using Raman spectrometer at room temperature. After the SERS measurement, SALDI-MS was carried out with the same Au-TNA substrate.

RESULTS AND DISCUSSION

Characterization of the Au−TNA Substrate. Titania nanotubes (TNA) have large free space in their interior and outer space that can be modified with metal such as gold and silver.[28−32] The highly orientated growth and uniform open-top characteristics of TNA provide potential to fabricate hot spots through nucleation and growth of metal nanoparticles to yield

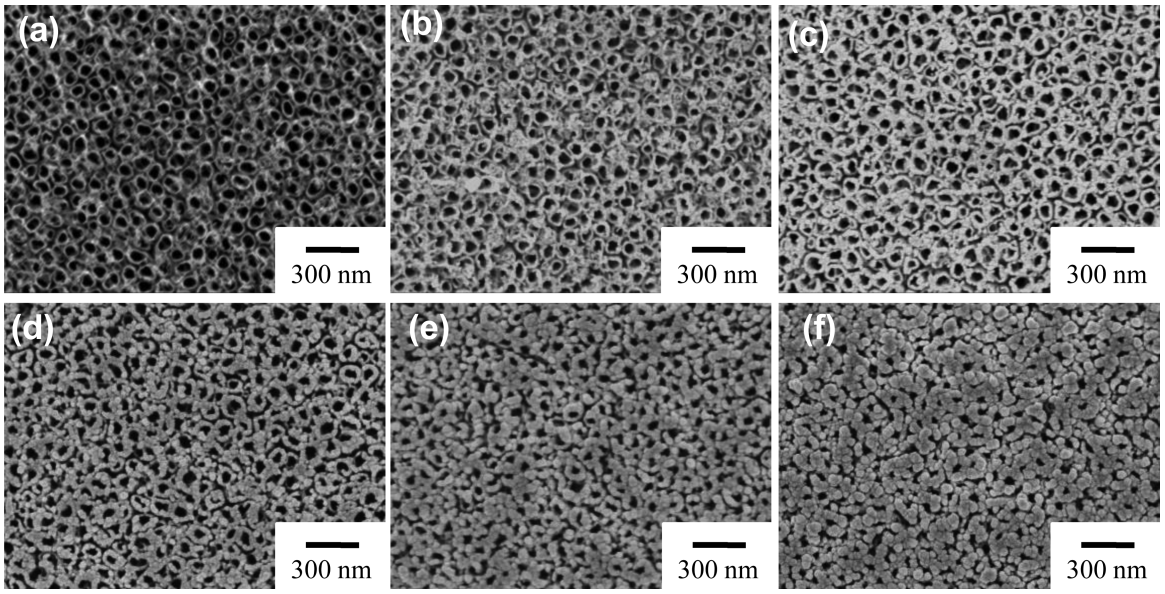

Figure 1. SEM images of the Au-TNA substrates (a) without Au and (b–f) covered with (b) 0.004, (c) 0.01, (d) 0.02, (e) 0.03, and (f) 0.04 mg/cm^2 Au.

high SERS performance. For example, a large SERS enhancement can be obtained using Ag nanoparticles deposited on TNA substrate.[32] In this study, we employed the Au-TNA substrate for a combined SERS and SALDI-MS analysis, since Au nanoparticles have higher SALDI activity than Ag nanoparticles.[33] The particle-like Au was deposited on TNA by MSVD. The Au-TNA substrate has local areas with high SERS enhancement, so-called hotspots,[34,35] induced by the aggregation of Au nanoparticles. Figure 1 shows SEM images of the Au-TNA substrates with various amounts of deposited Au (from 0.004 to 0.04 mg/cm^2). The Au morphology on the TNA depended on the amount of Au deposited. For less than 0.01 mg/cm^2 Au (Figure 1b, c), the Au nanoparticles with about 5–30 nm are located on the nanotube walls. The magnified SEM image of Au-TNA substrate with 0.01 mg/cm^2 Au is shown in Figure 2a. For the surface covered with more

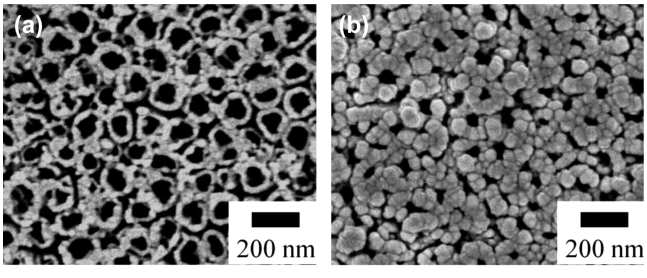

Figure 2. SEM images of the Au-TNA substrates: (a) 0.01 mg/cm^2 of Au (type I); (b) 0.04 mg/cm^{2}of Au (type II). The Au-TNA substrates with 0.04 mg/cm^{2}of Au show highly SERS activity, while that with 0.01 mg/cm^{2}of Au exhibit highly SALDI activity.

than 0.02 mg/cm^2 Au, the nanoparticle surface coverage increases (Figure 1d–f), resulting in agglomeration of the Au nanoparticles and the formation of granular Au film on the TNA. The tubular morphology is distorted because of the visible reduction of the internal diameter of the nanotubes in the TNA. The magnified SEM image of Au-TNA substrate with 0.04 mg/cm^2 Au is shown in Figure 2b. The size range of Au nanoparticles in granular Au film is 10–90 nm for 0.04 mg/cm^2 Au, as shown in a histogram of size distribution in Figure S1 in the Supporting Information.

The diffraction peaks of the Au crystals in the accompanying XRD spectra support the result (see Figure S2 in the Supporting Information), in that the peak intensities increased with increasing amounts of Au deposited on the TNA. The XRD spectra were further analyzed using Scherrer equation in order to determine average crystallite size of Au. The crystallite size of Au increased 37 nm for Au-TNA substrate with 0.004 mg/cm^2 to 164 nm for that with 0.04 mg/cm^2 (see Figure S3 in the Supporting Information). It should be noted that the crystallite size of Au from XRD spectra is much larger than the size of Au nanoparticles (see Figure S1 in the Supporting Information) from SEM images in the case of Au-TNA substrate with more than 0.02 mg/cm^2 Au. Therefore, it seems that Au particles on TNA are not on the form of isolated nanoparticles but granular film on the TNA for Au-TNA substrate with more than 0.02 mg/cm^2 Au.

On the basis of the above SEM observation and the XRD spectra, we tentatively define the two types of Au-TNA substrates with different Au morphologies depending on the amount of deposited Au: (I) substrates with less than 0.01 mg/cm^2 Au, in which the Au nanoparticles are located on the nanotube walls and the tubular morphology of TNA is clearly intact, and (II) substrates with more than 0.02 mg/cm^2 Au, in which Au particles on TNA are in the form of granular film with particle diameters of 50–100 nm. The morphology of the Au-TNA substrate had a significant influence on whether the substrate exhibited SERS activity or SALDI activity: type II substrates showed high SERS activity, whereas type I substrates exhibited high SALDI activity. The details of this behavior are described below.

SERS-Active Substrates. The SERS activity of the Au-TNA substrates was investigated using a model analyte, R6G, for different amounts of deposited Au. It was found that substrates with more than 0.02 mg/cm^2 Au (type II) had high SERS activities. As typical examples, the SERS spectra of R6G obtained using the Au-TNA substrates with 0.004, 0.01, 0.02, 0.03, and 0.04 mg/cm^2 Au are shown in Figure 3a. The

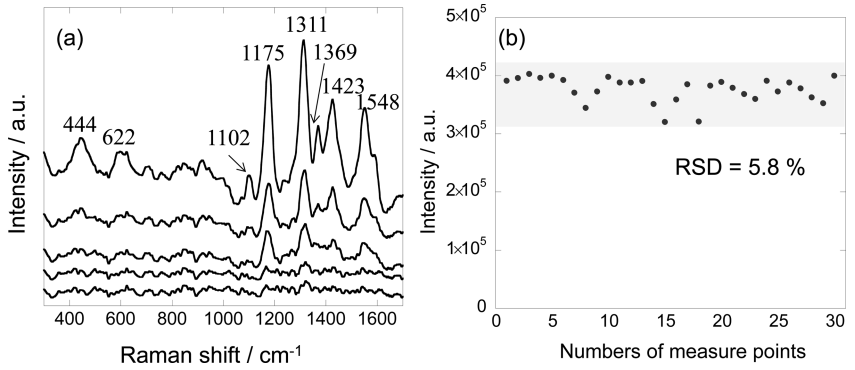

Figure 3. (a) SERS spectra of R6G on the Au-TNA substrates with 0.004, 0.01, 0.02, 0.03, and 0.04 mg/cm^2 Au from the bottom to the top. Before the SERS measurements, the Au-TNA substrates were immersed in 1 μM R6G aqueous solution. (b) SERS peak intensities of 4-ATP at 1070 cm^{-1} on the Au-TNA substrates with 0.04 mg/cm^2 of Au. The standard error obtained from 30 different locations is 5.8 % in the Raman signals. Before the SERS measurements, the Au-TNA substrates were immersed in 1 μM 4-ATP ethanol solution.

characteristic R6G bands at 444, 622, 1102, 1175, 1311, 1369, 1423, and 1548 cm^{-1} appear in the SERS spectra.[36,37] Assignment of the vibrational bands seen in the SERS spectra of R6G is shown in the Supporting Information, Table S1. In particular, large signals are achieved on the Au-TNA substrates with more than 0.04 mg/cm^2 Au, as shown in Figure S4 in the Supporting Information. The detection sensitivity for 4-ATP on the Au-TNA substrates with 0.04 mg/cm^2 was 10 nM in the SERS measurement (see Figure S5 in the Supporting Information). The AFM image of the Au-TNA substrate with 0.04 mg/cm^2 Au shows aggregated Au nanoparticles on the TNA (see Figure S6 in the Supporting Information), where the size of each nanoparticle on the granular film is about 50−100 nm. The large enhancement in the Raman signal obtained for these Au-TNA substrates presumably originates from the aggregated Au nanoparticles on the granular film, which may act as hot spots with extremely localized surface electromagnetic fields.[4−8,34,35] In addition, nanoparticles with sizes of 50−100 nm are well studied and have been shown to contribute to the high SERS activity. In particular, the highest SERS activity was observed for Au nanoparticles in the size range of 50−100 nm.[38,39] It is worthy of note that this SERS active-morphology of Au granular film can be obtained only for using the TNA substrate as the template. Instead, we also conducted the Au deposition on "un-etched titanium foil" under the similar MSVD condition as the case of the Au-TNA substrate. The Au-deposited titanium foil showed no formation of the Au granular film (Figure 4b), resulting in the very low SERS activity of 4-ATP (Figure 4a). This indicates that the combination of the TNA substrate with the MSVD deposition of Au nanoparticles can produce the SERS active-Au granular film on the TNA.

The reproducibility of the SERS measurements is also important for realizing commercial applications of SERS substrates. In order to evaluate the reproducibility of SERS measurements using Au-TNA substrates, the Raman signals of 4-ATP were again considered. It has been reported that 4-ATP molecule can be used for the characterization of the reproducibility of the SERS because of the formation of self-assembled monolayer of 4-ATP on gold surface via thiol-gold interaction.[40,41] For an excitation wavelength of λ = 785 nm, the resulting prominent spectral peaks were 1556, 1420, 1373, and 1135 cm^{-1}, which were assigned to the non-totally symmetric modes of the 4-ATP molecule.[42,43] Additional peaks were seen at 1170 and 1070 cm^{-1} and were assigned to

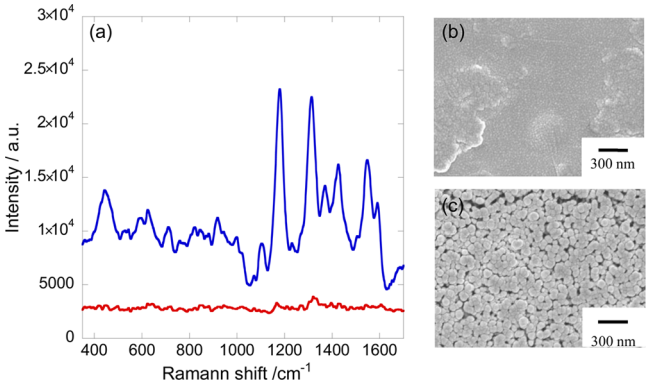

Figure 4. (a) SERS spectrum of R6G on Au deposited titanium foil with 0.06 mg/cm^2 Au (red line). (b) SEM image of the Au deposited titanium foil with 0.06 mg/cm^2 Au. For comparison, SERS spectrum of R6G (blue line) and (c) SEM image on Au TNA substrate with 0.06 mg/cm^2 Au are shown in panel a and image c, respectively. Before the SERS measurements, these substrates were immersed in 1 μM aqueous solution of R6G.

the totally symmetric modes. Herein, the strong Raman signal of 4-ATP at 1070 cm^{-1} was measured as the probe peak. The standard error (relative standard deviation; RSD) obtained from the Raman spectra of 4-ATP measured at 30 different locations was ~6 % (Figure 3b). Thus, the Au-TNA substrates prepared in our study have excellent spatial reproducibility and will be useful for commercial SERS applications. It should be noted that the area within 1 mm of the edge of the substrate was excluded in the SERS measurements, since the nanotube structures were deformed in the edge regions by the cutting from the original TNA substrate, resulting in poor spatial reproducibility.

SALDI-Active Substrates. The Au-TNA substrate can be also used as a SALDI substrate. We used angiotensin II (Ang. II) as the model analyte to evaluate the SALDI activity. Ang. II is a peptide that has often been used for the first screening of the SALDI activity, because it is known that ionization/desorption of the peptide cannot occur without LDI-assisting materials.[33] The Au-TNA substrate yielded protonated ions of Ang. II, $[M + H]^+$, as shown in Figure 5a. The peak intensities of Ang. II in the SALDI mass spectra as a function of the amount of Au deposited on the TNA substrates are shown in Figure 5b. The peak intensities of Ang. II are highest for the Au-TNA substrate with 0.01 mg/cm^2 Au (type I). On this

dx.doi.org/10.1021/am501291d | ACS Appl. Mater. Interfaces 2014, 6, 8387−8395

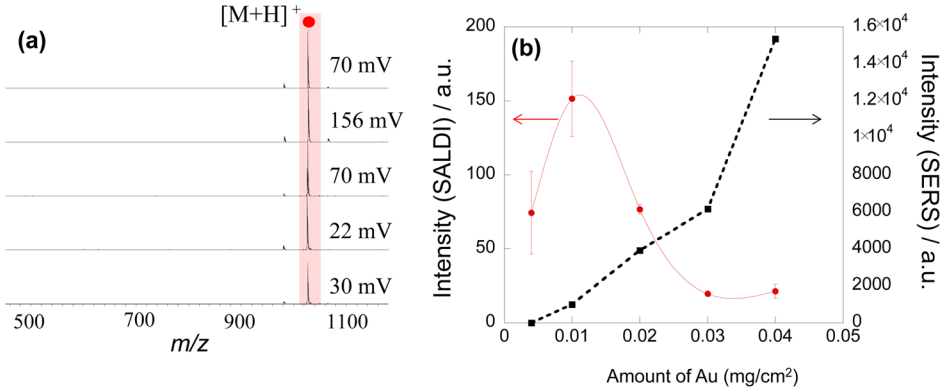

Figure 5. (a) SALDI mass spectra of Ang. II (5 pmol) obtained using the Au-TNA substrates covered with 0.004, 0.01, 0.02, 0.03, and 0.04 mg/cm^2 Au from the bottom to the top. The peak intensities (mV) are shown in the figure. (b) Effect of the amount of Au in the Au-TNA substrates on the SALDI peak intensity of Ang. II (red line). For comparison, the SERS intensity for R6G is also shown as a dotted line. Before the SERS measurements, the Au-TNA substrates were immersed in 1 μM R6G aqueous solution.

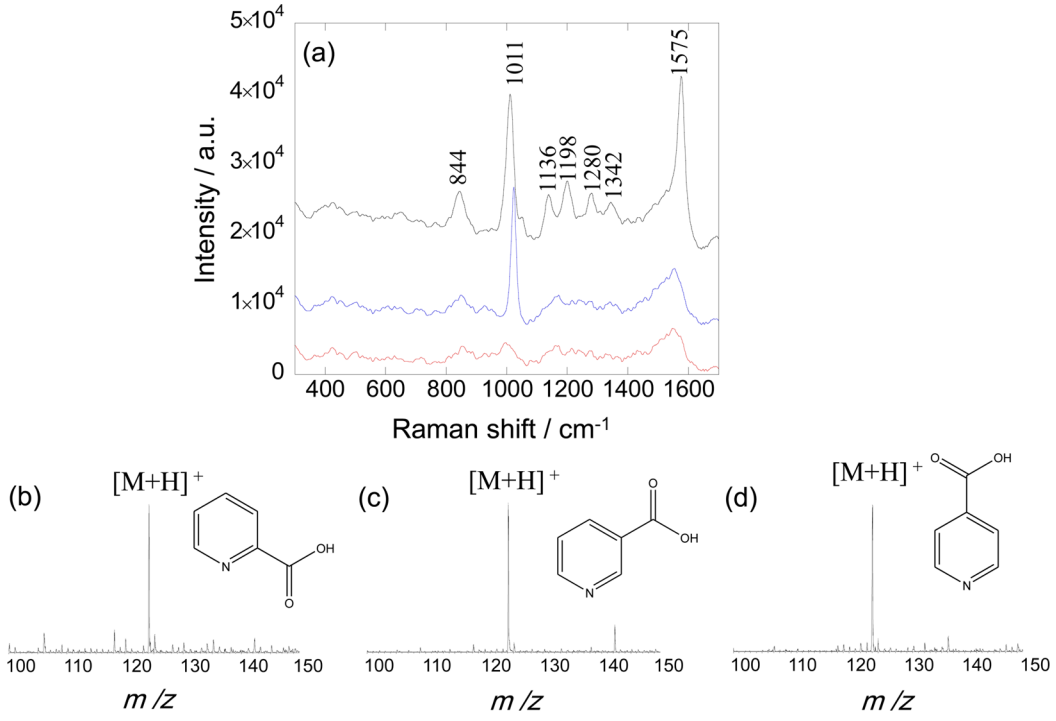

Figure 6. (a) SERS spectra of *p*-Py (black line), *m*-Py (blue line), and *o*-Py (red line) on the Au-TNA substrate with 0.04 mg/cm^2 Au. Before the SERS measurements, the Au-TNA substrates were immersed in 1 mM *p*-Py, *m*-Py, or *o*-Py aqueous solution. SALDI mass spectra of (b) *o*-Py, (c) *m*-Py, and (d) *p*-Py obtained using the Au-TNA substrate with 0.04 mg/cm^2 Au.

substrate, the Au nanoparticles are located on the nanotube walls, and the tubular morphology is clearly seen. However, the Au-TNA substrate with 0.01 mg/cm^2 Au showed very low SERS activity.

Although the SALDI mechanism has not been well clarified, it is most likely dominated by thermal processes due to laser-induced temperature increases during the short-pulse laser irradiation of the UV-absorbing nanoparticles in the SALDI-MS procedure.[13,19] The energy transfer from the metal nanoparticles to the analytes is likely thermally driven, which leads to more rapid temperature rises during laser light illumination than would be obtained without the metal nanoparticles. Our previous paper suggested that the heat diffusion length during the SALDI laser pulse is estimated to be about 100 nm.[33] To achieve the same temperature rise for the entire Au nanoparticle volume, the Au nanoparticles should be smaller than 100 nm in diameter. Thus, the Au nanoparticles larger than 100 nm and/or the large-scale agglomeration may lead to smaller temperature rises during the laser illumination, resulting on less SALDI activity for the type II substrates. In addition, the deformation of the tubular morphology of the TNA can reduce the SALDI activity for type II substrates, because the tubular morphology enhances the SALDI activity.[44]

Combined SERS and SALDI-MS Analysis with the Same Au-TNA Substrate. The above results indicate that optimal amounts of Au in the Au-TNA substrates for SERS and SALDI are different. The type II Au-TNA substrate with more than 0.02 mg/cm^2 Au showed better SERS activity, whereas the type I substrate with 0.01 mg/cm^2 Au showed high SALDI activity. Therefore, in this study, we selected an Au-TNA substrate with 0.04 mg/cm^2 Au for the combined SERS/SALDI analyses, although this substrate showed higher SERS activity

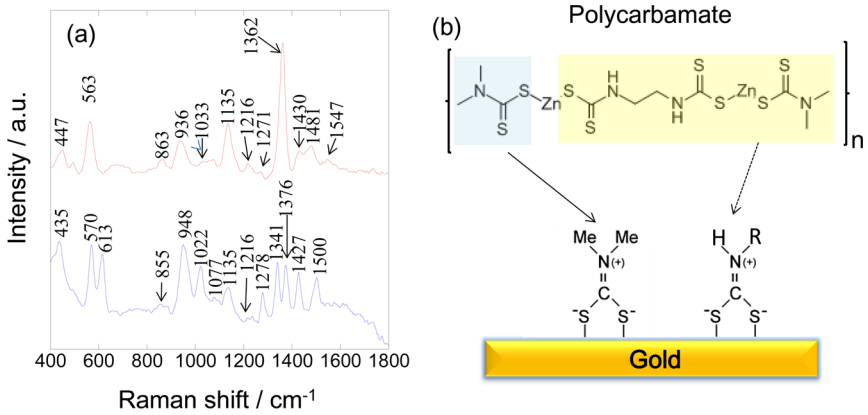

Figure 7. (a) SERS spectra of polycarbamate on the Au-TNA substrate with 0.04 mg/cm^2 Au (red line) and normal Raman spectrum of polycarbamate powder (blue line). (b) Schematic of the adsorption of polycarbamate on the gold surface.

than SALDI activity. Nevertheless, significant peak intensities in the SALDI-MS spectra were still observed for this Au-TNA substrate: the detection sensitivity for 4-ATP was 100 nM in the SALDI-MS measurement (see Figure S7 in the Supporting Information). The RSD value obtained from the peak of 4-ATP in the SALDI mass spectra at 50 different locations was ~18 % (see Figure S8 in the Supporting Information).

I. Pyridine Carboxylic Acid Isomers. The combined SERS and SALDI-MS analysis based on the Au-TNA substrates was carried out first for structural isomers of pyridine compounds. The SALDI mass spectra of *p*-Py, *m*-Py, and *o*-Py obtained using the Au-TNA substrates are shown Figure 6b–d, respectively. The protonated ions, $[M + H]^+$, were detected at *m/z* 124, but the mass spectra of all isomers were the same. Thus, SALDI-MS is capable of detecting the existence of pyridine carboxylic acid, but it is insufficient for isomer identification. On the other hand, the SERS analysis was successful in discriminating these three isomers. The SERS spectra of *p*-Py, *m*-Py, and *o*-Py are shown in Figure 6a. Assignment of the vibrational bands seen in the SERS spectra of *p*-Py, *m*-Py, and *o*-Py is shown in the Supporting Information, Table S2. In this experiment, we maintained a neutral to basic pH (7–9) for the sample solutions, since the carboxylate form adsorbs onto Au nanoparticles. In the case of *p*-Py, the characteristic carboxylate COO^- scissoring band is observed at 1342 cm^{-1}, and the COO^- symmetric stretching band is observed at 844 cm^{-1}. The characteristic band of carboxylate was also observed for *o*-Py and *m*-Py. The skeletal ring vibration bands of pyridine appear with a strong intensity around 1000 cm^{-1}, but the exact location depends on the isomer: the peak was at 1011, 1023, and 995 cm^{-1} for *p*-, *m*-, and *o*-Py, respectively. It was found that the ratio (R) of the peak intensity of the COO^- band (840–850 cm^{-1}) to that of the CC stretching band (1550–1570 cm^{-1}) also depended on the isomer: R = 1.1, 0.6, and 1.5 for *p*-, *m*-, and *o*-Py, respectively. Thus, it is concluded that (i) the skeletal ring vibration and (ii) the relative peak intensities can be used to discriminate the isomers of pyridine carboxylic acid in the SERS analysis. The chemical component of the overall SERS enhancement is associated with chemical interactions between the metal and the adsorbate, which can also affect the vibrational frequencies and intensities of the adsorbed molecules.[4–8] The isomers of pyridine carboxylic acids have the carboxylate and pyridine nitrogen at different relative positions, which may affect their orientations on the gold surface.[45] These different orientations should be detected as changes in the frequencies and intensities in the SERS spectra.

ii. Polycarbamate. Recently, the use of SERS techniques for ultrasensitive detection in environmental analysis has been the subject of intense research.[46] Here, we performed the first combined SERS and SALDI-MS analysis to detect polycarbamate, which is a dithiocarbamate fungicide (DTC) used in agriculture, in water. Although DTCs are broad-spectrum fungicides, they have been suspected of exhibiting teratogenic, carcinogenic, immunotoxic, and mutagenic effects.[47] Monomeric DTCs such as thiram and ziram can be detected sensitively by liquid chromatography (LC) with mass spectrometry (MS) and gas chromatography-mass spectrometry (GC-MS).[48–50] However, polymeric DTCs including polycarbamate are difficult to detect directly, because they are insoluble in general solvents. Thus, methods for detecting polycarbamate involve complex pre-treatments such as alkali decomposition and derivatization for analysis.[43–45] In contrast, the combined SERS and SALDI-MS analysis for the direct detection of polycarbamate in water requires no pre-treatment. Polycarbamate is hardly soluble in water, but the infinitesimal quantities adsorbed from the insoluble solid sample onto the gold surface may be sufficient for the detection with the highly sensitive SERS and SALDI techniques.

After the Au-TNA substrates were immersed into the supernatant of the polycarbamate suspension, the SERS spectrum of the Au-TNA substrate was obtained, as shown in Figure 7a (red line). For comparison, the normal Raman spectrum (i.e., not SERS) of polycarbamate powder is shown in Figure 7a (blue line). Although the SERS spectra of DTCs species obtained under a variety of analytical conditions have been reported before,[51–53]the peak assignments are still matter of debate for some vibrational modes. Here, tentative assignments for the bands highlighted have been made based on the peak locations previously reported in the literature.[51–53] The main Raman bands in the SERS spectrum are at 447 cm^{-1} for the δ_{CH3NC} + ν(C═S) mode; 936 cm^{-1} for $\nu(CH_3N)$ + ν(C═S); 1135 cm^{-1} for $\rho(CH_3)$ + ν(C–N); 1216 and 1271 cm^{-1} for the ν(CSS), ν(C–N), and δ(N–H) vibrations; 1362 cm^{-1} for $\delta_s(CH_3)$ + ν(C–N); 1430 cm^{-1} for δ_{as} (CH_3); and 1481 cm^{-1} for ν(C–N) + $\rho(CH_3)$. The SERS spectrum greatly differs from the normal Raman spectrum (i.e. no SERS) of polycarbamate powder. It is important to note that the intensities of the SERS peaks corresponding to the C═S modes are smaller than those in the normal Raman

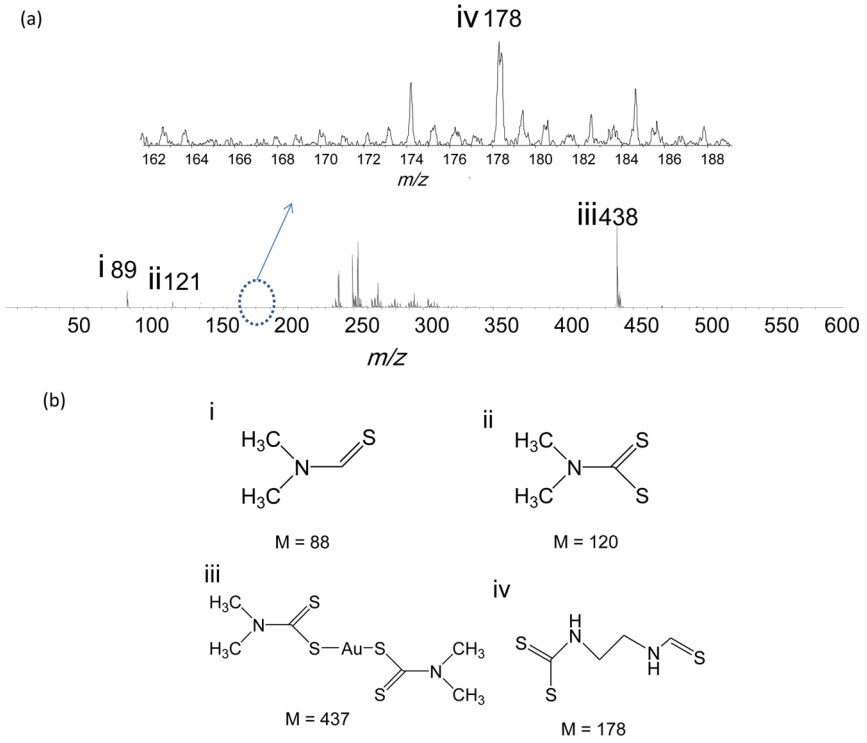

Figure 8. (a) SALDI mass spectra of polycarbamate on the Au-TNA substrate with 0.04 mg/cm^2 Au. (b) Possible assignments for SALDI mass spectra of polycarbamate on the Au-TNA substrate shown in Figure 6

spectrum from polycarbamate powder. It has been reported that the position of the ν(C−N) band at around 1500 cm^{-1} of DTCs could be used to estimate the strength of the interaction between this ligand and the metal.[53] The intensity of this band is lower in the SERS spectrum than in the normal Raman spectrum, and it is shifted to 1547 cm^{-1}, indicating an increase in the double bond character and, consequently, a strengthening of the interaction with the metal.[53] These changes in the spectrum suggest that polycarbamate may undergo a breakdown of the S−Zn−S bond, and the resultant resonant radical species interact with the gold surface to form dimethyldithiocarbamate and ethylenebisdithiocarbamate, as shown in Figure 7b.

We can also detect MS peaks from polycarbamate in the SALDI mass spectra. After the SERS measurement, the SALDI mass spectra were acquired using the same Au-TNA substrate, as shown in Figure 8. We cannot detect an intact, nonfragmented molecular ion of polycarbamate because of its limited stability. Alternatively, three fragment ions, *m/z* 89, 121, and 438 were observed, which were assigned to the protonated ions from the fragmentation of dimethyldithiocarbamate, as shown in Figure 8b. A minor peak at *m/z* 178 was also observed, presumably corresponding to the mass of ethylenebisdithiocarbamate (210) minus 32 (mass of S). Thus, this may be assigned to the ion from the fragmentation of ethylenebisdithiocarbamate. Because the peak intensities corresponding to ethylenebisdithiocarbamate are very small, it is possible that the desorption/ionization efficiency of ethylenebisdithiocarbamate in the SALDI-MS is lower than that of dimethyldithiocarbamate. It should be also noted that two unknown peaks were observed at *m/z* 556 and 492. The mass difference between these peaks is 64, which is consistent with the mass of "two sulfur" (see Figure S9 in the Supporting Information), implying that these unknown peaks might be dimer from polycarbamate.

The above results demonstrate that the adsorption of a sulfur-containing pesticide on the Au surface makes it possible to identify and detect this species using SERS/SALDI techniques with the Au-TNA substrates.

CONCLUSION

It was demonstrated that gold-decorated titania nanotube arrays (Au-TNA substrates) acted as dual-functional platforms for surface-enhanced Raman spectroscopy (SERS) and surface-assisted laser desorption/ionization mass spectrometry (SALDI-MS). The optimal amount of Au in the Au-TNA substrate to maximize the SALDI-MS and SERS was explored. In particular, the Au morphologies of Au-TNA substrates with different amounts of Au were found to significantly affect whether they exhibited SERS activity or SALDI activity: Au-TNA substrates with more than 0.02 mg/cm^2 Au (type II) showed high SERS activity, whereas those with 0.01 mg/cm^2 Au (type I) exhibited high SALDI activity. Excellent reproducibility of SERS was found for the optimized Au-TNA substrate, with a standard error of less than 6 %. With the same Au-TNA substrate, the SALDI activity was also demonstrated.

Combined SERS and SALDI-MS analysis using the Au-TNA substrate was demonstrated by (i) discriminating the structural isomers of pyridine compounds (para-, meta-, and ortho-pyridinecarboxylic acid) and (ii) detecting polycarbamate. The combined SERS and SALDI-MS analysis using Au-TNA substrates successfully discriminated the pyridine compound isomers: the compound can be identified from the mass in the SALDI-MS spectrum, and further isomer discrimination can be achieved by SERS analysis, because there are differences in the adsorbate−gold bonds among the isomer compounds.

dx.doi.org/10.1021/am501291d | ACS Appl. Mater. Interfaces 2014, 6, 8387−8395

Furthermore, the combined SERS and SALDI-MS technique was useful for the direct analysis of polycarbamate in water without pre-treatment. Polycarbamate is hardly soluble in water, but the infinitesimal quantities of polycarbamate adsorbed from the insoluble solid sample onto the gold surface were sufficient for the detection using the highly sensitive SERS and SALDI techniques. The synergy between these techniques makes analysis of analytes from the same location on the same sample possible.

■ ASSOCIATED CONTENT

Supporting Information

XRD spectra of the Au-TNA substrates; SEM and AFM images of the Au-TNA substrate; SERS spectra of 4-ATP on the Au-TNA substrates; SALDI mass spectra of 4-ATP on the Au-TNA substrates; assignment of the vibrational bands seen in the SERS spectra of R6G, *p*-Py, *m*-Py, and *o*-Py. This material is available free of charge via the Internet at http://pubs.acs.org.

■ AUTHOR INFORMATION

Corresponding Author

*E-mail: hkawa@kansai-u.ac.jp.

Notes

The authors declare no competing financial interest.

■ ACKNOWLEDGMENTS

This study was supported in part by the "Strategic Project to Support the Formation of Research Bases at Private Universities" with a matching Fund Subsidy from the Ministry of Education, Culture, Sports, Science and Technology (MEXT), Japan. This study was also partially supported by Grants-in-Aid for Scientific Research (Nos. 23360361, 23655074, and 22350040) from the Japan Society for the Promotion of Science (JSPS) and the Network Joint Research Center for Materials and Devices (2013A20).

■ REFERENCES

(1) Rycenga, M.; Cobley, C. M.; Zeng, J.; Li, W.; Moran, C. H.; Zhang, Q.; Qin, D.; Xia, Y. Controlling the Synthesis and Assembly of Silver Nanostructures for Plasmonic Applications. *Chem. Rev.* **2011**, *111*, 3669−3712.

(2) Halas, N. J.; Lal, S.; Chang, W. S.; Link, S.; Nordlander, P. Plasmons in Strongly Coupled Metallic Nanostructures. *Chem. Rev.* **2011**, *111*, 3913−3961.

(3) Jones, M. R.; Osberg, K. D.; Macfarlane, R. J.; Langille, M. R.; Mirkin, C. A. Templated Techniques for the Synthesis and Assembly of Plasmonic Nanostructures. *Chem. Rev.* **2011**, *111*, 3736−3827.

(4) Ko, H.; Singamaneni, S.; Tsukruk, V. V. Nanostructured Surfaces and Assemblies as SERS Media. *Small* **2008**, *4*, 1576−1599.

(5) Cialla, D.; März, A.; Böhme, R.; Theil, F.; Weber, K.; Schmitt, M.; Popp, J. Surface-enhanced Raman spectroscopy (SERS): Progress and Trends. *Anal. Bioanal. Chem.* **2012**, *403*, 27−54.

(6) Alvarez-Puebla, R. A.; Liz-Marzán, L. M. Traps and Cages for Universal SERS Detection. *Chem. Soc. Rev.* **2012**, *41*, 43−51.

(7) Gong, X.; Bao, Y.; Qiu, C.; Jiang, C. Individual Nanostructured Materials: Fabrication and Surface-Enhanced Raman Scattering. *Chem. Commun.* **2012**, *48*, 7003−7018.

(8) Abramczyk, H.; Brozek-Pluska, B. Raman Imaging in Biochemical and Biomedical Applications. Diagnosis and Treatment of Breast Cancer. *Chem. Rev.* **2013**, *113*, 5766−5781.

(9) Mayer, K. M.; Hafner, J. H. Localized Surface Plasmon Resonance Sensors. *Chem. Rev.* **2011**, *111*, 3828−3857.

(10) Lin, Y. W.; Huang, C. C.; Chang, H. T. Gold Nanoparticle Probes for the Detection of Mercury, Lead and Copper Ions. *Analyst* **2011**, *136*, 863−871.

(11) Saha, K.; Agasti, S. S.; Kim, C.; Li, X.; Rotello, V. M. Gold Nanoparticles in Chemical and Biological Sensing. *Chem. Rev.* **2012**, *112*, 2739−2779.

(12) Peterson, D. S. Matrix-free Methods for Laser Desorption/Ionization Mass Spectrometry. *Mass Spectrom. Rev.* **2007**, *26*, 19−34.

(13) Arakawa, R.; Kawasaki, H. Functionalized Nanoparticles and Nanostructured Surfaces for Surface-Assisted Laser Desorption/Ionization Mass Spectrometry. *Anal. Sci.* **2010**, *26*, 1229−1240.

(14) Law, K. P.; Larkin, J. R. Recent Advances in SALDI-MS Techniques and Their Chemical and Bioanalytical Applications. *Anal. Bioanal. Chem.* **2011**, *399*, 2597−2622.

(15) Chiang, C. K.; Chen, W. T.; Chang, H. T. Nanoparticle-Based Mass Spectrometry for the Analysis of Biomolecules. *Chem. Soc. Rev.* **2011**, *40*, 1269−1281.

(16) Greving, M. P.; Patti, G. J.; Siuzdak, G. Nanostructure-Initiator Mass Spectrometry Metabolite Analysis and Imaging. *Anal. Chem.* **2011**, *83*, 2−7.

(17) Pilolli, R.; Palmisano, F.; Cioffi, N. Gold Nanomaterials as a New Tool for Bioanalytical Applications of Laser Desorption Ionization Mass Spectrometry. *Anal. Bioanal. Chem.* **2012**, *402*, 601−623.

(18) Stolee, J. A.; Walker, B. N.; Zorba, V.; Russo, R. E.; Vertes, A. Laser−Nanostructure Interactions for Ion Production. *Phys. Chem. Chem. Phys.* **2012**, *14*, 8453−8471.

(19) Silina, Y. E.; Volmer, D. A. Nanostructured Solid Substrates for Efficient Laser Desorption/Ionization Mass Spectrometry (LDI-MS) of Low Molecular Weight Compounds. *Analyst* **2013**, *138*, 7053−7065.

(20) Nakamura, Y.; Tsuru, Y.; Fujii, M.; Taga, Y.; Kiya, A.; Nakashima, N.; Niidome, Y. Sensing of Oligopeptides using Localized Surface Plasmon Resonances Combined with Surface-Assisted Laser Desorption/Ionization Time-of-Flight Mass Spectrometry. *Nanoscale* **2011**, *3*, 3793−3798.

(21) Chen, J. Y.; Chen, Y. C. A Label-Free Sensing Method for Phosphopeptides Using Two-Layer Gold Nanoparticle-Based Localized Surface Plasma Resonance Spectroscopy. *Anal. Bioanal. Chem.* **2011**, *399*, 1173−1180.

(22) Inuta, M.; Arakawa, R.; Kawasaki, H. Use of Thermally Annealed Multilayer Gold Nanoparticle Films in Combination Analysis of Localized Surface Plasmon Resonance Sensing and MALDI Mass Spectrometry. *Analyst* **2011**, *136*, 1167−1176.

(23) Cyriac, J.; Li, G.; Cooks, R. G. Vibrational Spectroscopy and Mass Spectrometry for Characterization of Soft Landed Polyatomic Molecules. *Anal. Chem.* **2011**, *83*, 5114−5121.

(24) Nie, B.; Masyuko, R. N.; Bohn, P. W. Correlation of Surface-Enhanced Raman Spectroscopy and Laser Desorption-Ionization Mass Spectrometry Acquired from Silver Nanoparticle Substrates. *Analyst* **2012**, *137*, 1421−1427.

(25) Gong, D.; Grimes, C.; Varghese, O.; Hu, W.; Singh, R.; Chen, Z. Titanium Oxide Nanotube Arrays Prepared by Anodic Oxidation. *J. Mater. Res.* **2001**, *16*, 3331−3334.

(26) Macàk, J. M.; Tsuchiya, H.; Schmuki, P. Smooth Anodic TiO_2 Nanotubes. *Angew. Chem., Int. Ed.* **2005**, *44*, 7463−7465.

(27) Elmoula, M. A.; Panaitescu, E.; Phan, M.; Yin, D.; Richter, C.; Lewis, L. H.; Menon, L. Controlled Attachment of Gold Nanoparticles on Ordered Titania Nanotube Arrays. *J. Mater. Chem.* **2009**, *19*, 4483−4487.

(28) Rani, S.; Roy, S. C.; Paulose, M.; Varghese, O. K.; Mor, G. K.; Kim, S.; Yoriya, S.; LaTempa, T. J.; Grimes, C. A. Synthesis and Applications of Electrochemically Self-Assembled Titania Nanotube Arrays. *Phys. Chem. Chem. Phys.* **2010**, *12*, 2780−2800.

(29) Mohamed, A. E. R.; Rohani, S. Modified TiO_2 Nanotube Arrays (TNTAs): Progressive Strategies Towards Visible Light Responsive Photoanode, a Review. *Energy Environ. Sci.* **2011**, *4*, 1065−1086.

(30) Huang, J. Y.; Zhang, K. Q.; Lai, Y. K. Fabrication, Modification, and Emerging Applications of TiO_2 Nanotube Arrays by Electrochemical Synthesis: A Review. *Int. J. Photoenergy* **2013**, *2013*, Article ID 761971, 19 page.

(31) Xiao, P.; Zhang, Y.; Garcia, B. B.; Sepehri, S.; Liu, D.; Cao, G. Nanostructured Electrode with Titania Nanotube Arrays: Fabrication, Electrochemical Properties, and Applications for Biosensing. *J. Nanosci. Nanotechnol.* **2009**, *9*, 2426−2436.
(32) Roguska, A.; Kudelski, A.; Pisarek, M.; Opara, M.; Janik-Czachor, M. Raman Investigations of SERS Activity of Ag Nanoclusters on a TiO_2-nanotubes/Ti Substrate. *Vib. Spectrosc.* **2011**, *55*, 38−43.
(33) Yonezawa, T.; Kawasaki, H.; Tarui, A.; Watanabe, T.; Arakawa, R.; Shimada, T.; Mafuné, F. Detailed Investigation on Possibility of Nanoparticles of Various Metal Elements for Surface-Assisted Laser Desorption/Ionization Mass Spectrometry. *Anal. Sci.* **2009**, *25*, 339−346.
(34) Lee, K.; Irudayaraj, J. Periodic and Dynamic 3-D Gold Nanoparticle−DNA Network Structures for Surface-Enhanced Raman Spectroscopy-Based Quantification. *J. Phys. Chem. C* **2009**, *113*, 5980−5983.
(35) Sheng, P.; Wu, S.; Bao, L.; Wang, X.; Chen, Z.; Cai, Q. Surface Enhanced Raman Scattering Detecting Polycyclic Aromatic Hydrocarbons with Gold Nanoparticle-Modified TiO_2 Nanotube Arrays. *New J. Chem.* **2012**, *36*, 2501−2505.
(36) Que, R. H.; Shao, M. W.; Zhuo, S. J.; Wen, C. Y.; Wang, S. D.; Lee, S. T. Highly Reproducible Surface-Enhanced Raman Scattering on a Capillarity-Assisted Gold Nanoparticle Assembly. *Adv. Funct. Mater.* **2011**, *21*, 3337−3343.
(37) Ding, Q.; Liu, H.; Yang, L.; Liu, J. Speedy and Surfactant-Free in Situ Synthesis of Nickel/Ag Nanocomposites for Reproducible SERS Substrates. *J. Mater. Chem.* **2012**, *22*, 19932−19939.
(38) Driskell, J. D.; Lipert, R. J.; Porter, M. D. Labeled Gold Nanoparticles Immobilized at Smooth Metallic Substrates:Systematic Investigation of Surface Plasmon Resonance and Surface-Enhanced Raman Scattering. *J. Phys. Chem. B* **2006**, *110*, 17444−17451.
(39) SeoHong, S.; Li, X. Optimal Size of Gold Nanoparticles for Surface-Enhanced Raman Spectroscopy under Different Conditions. *J. Nanomaterials* **2013**, *2013*, Article ID 790323, 9 pages.
(40) Tanoue, Y.; Sugawa, K.; Yamamuro, T.; Akiyama, T. Densely Arranged Two-Dimensional Silver Nanoparticle Assemblies with Optical Uniformity Over Vast Areas as Excellent Surface-Enhanced Raman Scattering Substrates. *Phys. Chem. Chem. Phys.* **2013**, *15*, 15802−15805.
(41) Perumal, J.; Voon Kong, K.; Dinish, U. S.; Bakker, R. M.; Olivo, M. Design and Fabrication of Random Silver Films as Substrate for SERS Based Nano-Stress Sensing of Proteins. *RSC Adv.* **2014**, *4*, 12995−13000.
(42) Kim, K.; Lee, H. S. Effect of Ag and Au Nanoparticles on the SERS of 4-Aminobenzenethiol Assembled on Powdered Copper. *J. Phys. Chem. B* **2005**, *109*, 18929−18934.
(43) Kim, K.; Yoon, J. K. Raman Scattering of 4-Aminobenzenethiol Sandwiched between Ag/Au Nanoparticle and Macroscopically Smooth Au Substrate. *J. Phys. Chem. B* **2005**, *109*, 20731−20736.
(44) Lo, C. Y.; Lin, J. Y.; Chen, W. Y.; Chen, C. T.; Chen, Y. C. Surface-Assisted Laser Desorption/Ionization Mass Spectrometry on Titania Nanotube Arrays. *J. Am. Soc. Mass. Spectrom.* **2008**, *19*, 1014−1020.
(45) Dressler, D. H.; Mastai, Y.; Rosenbluh, M.; Fleger, Y. Surface-Enhanced Raman Spectroscopy as a Probe for Orientation of Pyridine Compounds on Colloidal Surfaces. *J. Mol. Struct.* **2009**, *935*, 92−96.
(46) Álvarez-Puebla, R. A.; Liz-Marzán, L. M. Environmental Applications of Plasmon Assisted Raman Scattering. *Energy Environ. Sci.* **2010**, *3*, 1011−1017.
(47) Vettorazzi, G.; Almeida, W.; Burin, G. J.; Jaeger, R. B.; Robert, B.; Puga, F. R.; Rahde, A. F.; Reyes, F. G.; Schvartsman, S. International Safety Assessment of Pesticides: Dithiocarbamate Pesticides, ETU, and PTU—A Review and Update. *Teratog., Carcinog., Mutagen* **1995**, *15*, 313−337.
(48) Blasco, C.; Font, G.; Pico, Y. Determination of Dithiocarbamates and Metabolites in Plants by Liquid Chromatography−Mass Spectrometry. *J. Chromatogr. A* **2004**, *1028*, 267−276.
(49) Kawamoto, T.; Yano, M.; Makihata, N. Development of a High-Sensitivity Quantitative Analytical Method for Determining Polycarbamate by Gas Chromatography-Mass Spectrometry Incorporating Temperature-Programmable Inlet On-Column Injection. *J. Chromatogr. A* **2004**, *1074*, 155−161.
(50) Hayama, T.; Yada, K.; Onimaru, S.; Yoshida, H.; Todoroki, K.; Nohta, H.; Yamaguchi, M. Simplified Method for Determination of Polycarbamate Fungicide in Water Samples by Liquid Chromatography with Tandem Mass Spectrometry Following Derivatization with Dimethyl sulfate. *J. Chromatogr. A* **2007**, *1141*, 251−258.
(51) Saute, B.; Narayanan, R. Solution-Based Direct Readout Surface Enhanced Raman Spectroscopic (SERS) Detection of Ultra-Low Levels of Thiram with Dogbone Shaped Gold Nanoparticles. *Analyst* **2011**, *136*, 527−532.
(52) Wang, B.; Zhang, L.; Zhou, X. Synthesis of Silver Nanocubes as a SERS Substrate for the Determination of Pesticide Paraoxon and Thiram. *Spectrochim. Acta, Part A* **2014**, *121*, 63−69.
(53) Sánchez-Cortés, S.; Vasina, M.; Francioso, O.; Garćia-Ramos, J. V. Raman and Surface-Enhanced Raman Spectroscopy of Dithiocarbamate Fungicides. *Vib. Spectrosc.* **1998**, *17*, 133−144.